Applied Catalysis B: Environmental 163 (2015) 313–322

Contents lists available at ScienceDirect

Applied Catalysis B: Environmental

journal homepage: www.elsevier.com/locate/apcatb

# $Pt/Ce_xPr_{1-x}O_2$ ($x = 1$ or 0.9) $NO_x$ storage–reduction (NSR) catalysts

Verónica Rico-Pérez[a], Agustín Bueno-López[a,*], Dae Jung Kim[b], Yaying Ji[b], Mark Crocker[b,*]

[a] Department of Inorganic Chemistry, University of Alicante, Ap. 99, E-03080 Alicante, Spain
[b] Center for Applied Energy Research, University of Kentucky, KY 40511, USA

ARTICLE INFO

*Article history:*
Received 16 June 2014
Received in revised form 7 August 2014
Accepted 9 August 2014
Available online 17 August 2014

*Keywords:*
$NO_x$ storage reduction
Ceria
Doped ceria
Praseodymium
Pt–ceria interaction

ABSTRACT

Model $Pt/Ce_{0.9}Pr_{0.1}O_2$ and $Pt/CeO_2$ $NO_x$ storage–reduction catalysts were prepared via nitrate calcination, co-precipitation and carbon-templating routes. Raman spectroscopic data obtained on the catalysts indicated that the introduction of praseodymium into the ceria lattice increased the concentration of defect sites (vacancies), arising from the higher reducibility of the $Pr^{4+}$ cation compared to $Ce^{4+}$. For the Pr-promoted samples, $H_2$-TPR profiles contained high temperature bulk reduction peaks which were less pronounced compared with their ceria analogs, indicating that the presence of praseodymium enhances oxygen mobility due to the creation of lattice defects. Under lean-rich cycling conditions, the cycle-averaged $NO_x$ conversion of the $Pt/Ce_{0.9}Pr_{0.1}O_2$ samples was in each case substantially higher than that of the $Pt/CeO_2$ analog, amounting to a difference of 10–15% in the absolute $NO_x$ conversion in some cases. According to DRIFTS data, a double role can be assigned to Pr doping; on the one hand, Pr accelerates the oxidation of adsorbed $NO_x$ species during the lean periods. On the other hand, Pr doping destabilizes the adsorbed $NO_x$ species during the rich periods, and the kinetics of nitrate decomposition are faster on $Pt/Ce_{0.9}Pr_{0.1}O_2$, leading to improved catalyst regeneration. These results suggest that ceria-based mixed oxides incorporating Pr are promising materials for $NO_x$ storage–reduction catalysts intended for low temperature operation.



## 1. Introduction

The control of $NO_x$ emissions from lean-burn engines represents an on-going challenge to the automotive industry, particularly at the low exhaust temperatures associated with modern, fuel-efficient engines. As has been well documented elsewhere [1,2], two main technologies are currently used to reduce lean $NO_x$ emissions from mobile sources. Selective catalytic reduction (SCR) relies on the use of externally added urea which decomposes in situ to $CO_2$ and $NH_3$, the latter functioning as an excellent reductant for $NO_x$ in the presence of a suitable catalyst. The other main technology applied utilizes so-called Lean $NO_x$ Trap (LNT) catalysts, also known as $NO_x$ storage–reduction (NSR) catalysts, and relies on the storage of $NO_x$ on the catalyst as nitrites/nitrates; typically the $NO_x$ storage component of the catalyst is an alkali metal or alkaline earth oxide (most often BaO). Periodic rich operation of the engine induces release of the stored $NO_x$, which undergoes reduction on precious metal sites on the catalyst by the reductants present in the rich exhaust gas.

In previous studies on $NO_x$ reduction over NSR catalysts, the incorporation of ceria in NSR catalyst formulations has been shown to provide a range of benefits. Ceria can act as a support material and is particularly effective at stabilizing high Pt dispersions [3], in addition to BaO [4]. Moreover, ceria is able to store $NO_x$ at low to moderate temperatures [5–10], thereby improving NSR $NO_x$ storage capacity. This makes ceria-containing catalysts particularly attractive for relatively low temperature applications, given that BaO-based formulations typically perform poorly at temperatures below 250 °C [9]. The presence of ceria has also been shown by some workers to be beneficial for the $NO_x$ reduction function of NSR catalysts [5,6,8,11,12], and for increasing the selectivity of $NO_x$ reduction to $N_2$ (rather than $NH_3$) [11–14]. Ceria-containing catalysts also exhibit improved properties with respect to their sulfation–desulfation behavior [15,16], arising from the fact that ceria is able to store sulfur in the form of sulfate, the resulting cerium sulfates being less stable than alkaline earth sulfates [17].

In catalytic applications, ceria is frequently doped with rare earth elements in order to modify its electronic and/or structural

* Corresponding authors. Tel.: +1 859 257 0295; fax: +1 859 257 0220 (M. Crocker); Tel.: +34 600948665; fax: +34 965903454 (A. Bueno-Lopez).
*E-mail addresses:* agus@ua.es (A. Bueno-López), mark.crocker@uky.edu (M. Crocker).

http://dx.doi.org/10.1016/j.apcatb.2014.08.016
0926-3373/

properties. In the case that trivalent cations are incorporated into the $CeO_2$ lattice, anion vacancies are created by a charge-compensating effect, resulting in an increase in oxygen-storage capacity (OSC). These vacancies are associated with the dopant cations and are randomly distributed on anion sites within the fluorite lattice [18]. If the dopant has variable oxidation state, as is the case with praseodymium, the resulting vacancies are extremely mobile. This strongly influences the redox properties of the ceria by increasing both total and kinetic oxygen storage [19].

In view of the foregoing, we reasoned that the addition of praseodymium to ceria should be beneficial for $NO_x$ storage–reduction applications. Indeed, a study by Rohart and co-workers [20] found that doping 8 wt% Pr into a Ce–Zr mixed oxide resulted in a significant increase in the efficiency of $NO_x$ storage (for samples loaded with 1 wt% Pt), particularly at lower temperatures (200–350 °C). This increase was found to correlate with improved activity for NO oxidation over this temperature range. However, despite this promising result, there do not appear to have been any other reports concerning the properties of Ce–Pr mixed oxides in $NO_x$ storage–reduction. Therefore, in this study we prepared model $Pt/Ce_{0.9}Pr_{0.1}O_2$ catalysts via several different routes and, for comparison purposes, the $Pt/CeO_2$ analogs. In this paper we report their micro-structural properties, reduction behavior, and catalytic properties under $NO_x$ storage–reduction cycling.

## 2. Experimental

### 2.1. Catalyst preparation

$Pt/CeO_2$-M and $Pt/Ce_{0.9}Pr_{0.1}O_2$-M catalysts were prepared, where M indicates the synthesis method of the ceria-based support: N (nitrate calcination), C (activated carbon template) and U (homogeneous precipitation with urea). $Ce(NO_3)_3{\cdot}6H_2O$ (Alfa-Aesar, 99.99%), $Pr(NO_3)_3{\cdot}6H_2O$ (Sigma–Aldrich, 99.9%) and $Pt(NH_3)_4(NO_3)_2$ (Sigma–Aldrich, >50% Pt basis) were used as precursors.

#### 2.1.1. Support preparation by nitrate calcination

Powder $CeO_2$-N and $Ce_{0.9}Pr_{0.1}O_2$-N were prepared by heating pure $Ce(NO_3)_3{\cdot}6H_2O$ or $Ce(NO_3)_3{\cdot}6H_2O$ mixed with $Pr(NO_3)_3{\cdot}6H_2O$ in a 9:1 molar ratio, respectively, in a muffle furnace (static air) from room temperature to 500 °C at 10 °C/min, and maintaining the temperature at this value for 90 min [21].

#### 2.1.2. Support preparation with an activated carbon template

Darco KB-B activated carbon (Sigma–Aldrich) was dried in a vacuum oven at 100 °C overnight before use. $CeO_2$-C and $Ce_{0.9}Pr_{0.1}O_2$-C preparations were based on the method of Schüth et al. [22], which was modified by Crocker et al. [23]. The activated carbon template was gently stirred for 1 h in a 3.5 M aqueous solution of pure $Ce(NO_3)_3{\cdot}6H_2O$ or $Ce(NO_3)_3{\cdot}6H_2O$ mixed with $Pr(NO_3)_3{\cdot}6H_2O$ in a 9:1 molar ratio, using a twofold volumetric excess of solution based on the pore volume of the carbon. The resulting slurry was filtered on a Büchner funnel under suction. To remove residual liquid on the surface of the carbon, the product was sandwiched between sheets of filter paper and gently squeezed. The solid product was calcined in air in a muffle furnace using a heating rate of 5 °C/min from room temperature up to 250 °C, was held at this temperature for 30 min (to slowly combust the carbon template), and then calcined at 500 °C for 90 min using a heating ramp of 10 °C/min.

#### 2.1.3. Support preparation by homogeneous precipitation with urea

$Ce_{0.9}Pr_{0.1}O_2$-U and $CeO_2$-U were prepared following the method of Jacobs et al. [24]. The appropriate amounts of $Pr(NO_3)_3{\cdot}6H_2O$ and/or $Ce(NO_3)_3{\cdot}6H_2O$ were mixed with urea (Alfa Aesar 98+%) and dissolved in deionized water. $NH_4OH$ (Alfa Aesar, 28–30% $NH_3$) was then added dropwise (~1 mL/min). 6 g of urea, 30 mL $H_2O$ and 1 mL $NH_4OH$ were used per gram of metal oxide product obtained. The mixture was then heated at 90 °C with constant stirring overnight. The resulting precipitate was filtered, washed with boiling deionized water, and dried in a vacuum oven at 100 °C overnight. The dried precipitate was then crushed and calcined in a muffle furnace at 500 °C for 90 min using a heating ramp of 10 °C/min.

#### 2.1.4. Platinum loading by incipient wetness impregnation

Platinum was loaded on $CeO_2$ and $Ce_{0.9}Pr_{0.1}O_2$ powder supports by incipient wetness impregnation using an aqueous solution of $Pt(NH_3)_4(NO_3)_2$ in the appropriate concentration to obtain 1 wt% of metal loading. The impregnated supports were placed in a muffle furnace held at 250 °C (flash calcination); once introduced, the temperature was raised to 500 °C using a heating rate of 10 °C/min and held at this value for 30 min.

### 2.2. Catalyst characterization

X-ray diffractograms of the catalysts were recorded on a Phillips X'Pert diffractometer using Cu$K\alpha$ radiation ($\lambda = 1.540598$ Å). Diffractograms were recorded between 5° and 90° ($2\theta$) with steps of 0.017° and a step time of 50 s. The average crystal size ($D$) of the ceria-based supports was determined using the Scherrer equation [25].

Raman spectra of the catalysts were recorded using a Jobin Yvon Horiba Raman dispersive spectrometer with a variable-power He–Ne laser source (632.8 nm), equipped with a confocal microscope with a 10× objective of long focal length. The spectrum of each sample was obtained as the average signal of two individual spectra of different areas of the sample. The acquisition time for each individual spectrum was 20 s. The detector was of the CCD cooled Peltier type.

$N_2$ adsorption and desorption isotherms were obtained at −196 °C in a Micromeritics Tri-star system. Prior to the $N_2$ adsorption measurements the catalysts were outgassed at 160 °C overnight under vacuum. The obtained isotherms were used to determine the BET specific surface areas and pore volumes of the catalysts.

X-ray photoelectron spectroscopy (XPS, K-ALPHA, Thermo Scientific) was used to analyze the surfaces of the catalysts. All spectra were collected using Al-K$\alpha$ radiation (1486.6 eV), monochromatized by a twin crystal monochromator, yielding a focused X-ray spot with a diameter of 400 μm, at 3 mA × 12 kV. The alpha hemispherical analyser was operated in the constant energy mode with a pass energy of 50 eV. Charge compensation was achieved with a low energy electron flood gun and low energy argon ions from a single source.

Pt dispersion was calculated by $H_2$ chemisorption at dry ice temperature (−78 °C) in a Micromeritics AutoChem II Analyzer, which was equipped with a Thermal Conductivity Detector (TCD) to monitor $H_2$ uptake. A cold trap, consisting of a mixture of isopropyl alcohol and dry ice, was used to cool the samples. The catalysts (1 g) were first pretreated in a 10% $O_2$/He gas flow for 15 min at 400 °C, and were reduced afterwards with 10% $H_2$/Ar for 15 min at 300 °C. Subsequently, they were heated to 400 °C (hold time 10 min) in flowing Ar to remove adsorbed hydrogen. After the catalysts were cooled to −78 °C, $H_2$ pulses (0.5 mL of 10% $H_2$/Ar every 2 min) were introduced using a four-way valve. The $H_2$ signal at the reactor outlet was monitored by means of the TCD detector. $H_2$ pulsing was terminated after the TCD signal had reached a constant value, i.e., when the Pt sites were saturated with $H_2$. Assuming a 1:1 ratio of atomic hydrogen to surface Pt, the metal dispersion was calculated based on the amount of H adsorbed [26].

**Table 1**
Gas composition used for cycling ($NO_x$ storage/reduction) experiments.

| Parameter | Lean | Rich |
|---|---|---|
| Duration (s) | 120 | 10 |
| Temperature (°C) | 200, 300, 400 | 200, 300, 400 |
| Space velocity ($h^{-1}$) | 30,000 | 30,000 |
| NO (ppm) | 300 | 0 |
| $O_2$ (%) | 5 | 0 |
| $H_2$ (%) | 0 | 1.34 |
| CO (%) | 0 | 4 |
| $H_2O$ (%) | 5 | 5 |
| $CO_2$ (%) | 5 | 5 |
| He (%) | Balance | Balance |

Temperature programmed reduction with $H_2$ ($H_2$-TPR) of the catalysts was also carried out in a Micromeritics AutoChem II Analyzer. 150 mg of fresh catalyst was pretreated in situ at 150 °C for 1 h in a 50 mL/min Ar flow to remove adsorbed water. After cooling to room temperature, the gas flow was switched to 50 mL/min of 10% $H_2$ in Ar and the temperature was increased at 10 °C/min up to 900 °C.

### 2.3. $NO_x$ storage efficiency experiments

Experiments to determine the $NO_x$ storage efficiency (NSE) of the catalysts were performed in a microreactor using a mass spectrometer (Pfeiffer OmniStar) as the detector. Prior to measurements, the catalyst (ca. 0.15 g) was pretreated at 450 °C in flowing 10% $H_2$/Ar for 1 h, purged with Ar and cooled down to 200 °C. All gas flows were set to give a Gas Hourly Space Velocity (GHSV) of 30,000 $h^{-1}$. The NSE was measured at 200 °C by exposing the catalyst to flowing gas containing 300 ppm NO, 5% $O_2$, 5% $CO_2$, 3.5% $H_2O$, and balance He. The NSE was calculated from Eq. (1), where $t$ represents the duration of the storage phase:

$$\mathrm{NSE} = \frac{\int_0^t (\mathrm{NO}_{x,\ \mathrm{in}} - \mathrm{NO}_{x,\ \mathrm{out}})\,\mathrm{d}t}{\int_0^t \mathrm{NO}_{x,\ \mathrm{in}}\,\mathrm{d}t} \times 100\% \quad (1)$$

### 2.4. Catalyst tests under cycling conditions

Catalyst tests were performed using a quartz reactor tube loaded with ca. 0.14 g of catalyst powder. Effluent gases were analyzed online using a mass spectrometer (Pfeiffer OmniStar). All (lean and rich) flow conditions were operated at a GHSV of 30,000 $h^{-1}$. Before each experiment the catalyst was pretreated in 60 mL/min of 10% $H_2$/Ar flow at 450 °C for 1 h. $NO_x$ storage–regeneration experiments were performed while cycling between lean and rich conditions. Following pre-treatment, the catalyst was cooled or warmed to the measurement temperature, after which lean-rich cycling was performed until the catalyst reached a cycle-average steady state. The cycling parameters and gas composition used for the cycling experiments are summarized in Table 1. Once "stationary" concentration cycles had been established, the $NO_x$ concentration was averaged over five lean-rich cycles to give a mean conversion according to the following formula, where $t$ represents the duration of the combined lean and rich phases:

$$\mathrm{NO}_x \ \ \mathrm{conversion} = \frac{\int_0^t (\mathrm{NO}_{x,\ \mathrm{in}} - \mathrm{NO}_{x,\ \mathrm{out}})\mathrm{d}t}{\int_0^t \mathrm{NO}_{x,\ \mathrm{in}}\mathrm{d}t} \times 100\% \quad (2)$$

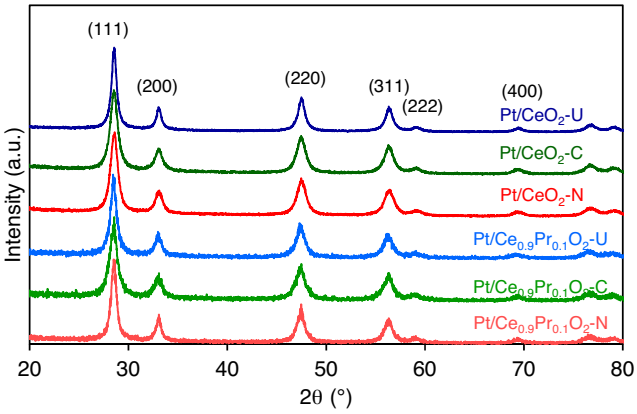


**Fig. 1.** XRD patterns of the catalysts.

### 2.5. DRIFTS measurements

DRIFTS measurements were performed using a Nicolet 6700 IR spectrometer equipped with a Harrick Praying Mantis accessory and MCT detector. The temperature of the reactor cell was controlled and monitored by a K-type thermocouple placed beneath the reaction chamber. For each DRIFT spectrum an average of 115 scans was collected (requiring ca. 1 min) with a resolution of 4 $cm^{-1}$. Catalyst samples were pretreated in situ in flowing 1% $H_2$/Ar at 400 °C for 1 h, followed by purging with Ar at 500 °C for 1 h. Samples were then cooled to 200 °C in flowing Ar, background spectra being collected at this temperature. $NO_x$ storage was carried out at 200 °C using a feed consisting of 300 ppm NO, 5% $O_2$ and Ar (balance). During $NO_x$ storage spectra were collected as a function of time. After 30 min of $NO_x$ storage, the feed gas was switched to 1% $H_2$ in Ar, DRIFT spectra again being recorded at regular intervals.

## 3. Results and discussion

### 3.1. X-ray diffraction, $N_2$ adsorption at −196 °C and Raman spectroscopy characterization

XRD patterns of the prepared catalysts are compiled in Fig. 1, showing the characteristic reflections of the $CeO_2$ fluorite structure corresponding to (1 1 1), (2 0 0), (2 2 0), (3 1 1), (2 2 2) and (4 0 0) planes [27]. Diffraction peaks attributed to Pt metal or platinum oxides [28–30] were not observed, indicating that the Pt species must be highly dispersed.

Table 2 includes the BET surface area and pore volume of the catalysts and also the crystal size and lattice parameter corresponding to the ceria-based supports, determined by $N_2$

**Table 2**
$N_2$ adsorption and XRD characterization results.

| Sample | BET surface area ($m^2$/g) | Single point ADS pore volume ($cm^3$/g) | Crystal size (nm) | Lattice parameter (nm) |
|---|---|---|---|---|
| Pt/$CeO_2$-U | 79 | 0.10 | 14 | 0.541 |
| Pt/$CeO_2$-C | 93 | 0.21 | 9 | 0.541 |
| Pt/$CeO_2$-N | 79 | 0.24 | 10 | 0.540 |
| Pt/$Ce_{0.9}Pr_{0.1}O_2$-U | 87 | 0.09 | 13 | 0.543 |
| Pt/$Ce_{0.9}Pr_{0.1}O_2$-C | 92 | 0.22 | 10 | 0.541 |
| Pt/$Ce_{0.9}Pr_{0.1}O_2$-N | 49 | 0.20 | 12 | 0.542 |

**Table 3**
Atomic surface concentration determined by XPS (concentrations in at.%).

| Sample | C | Pt | O | Ce | Pr | Ce/Pr[a] | Pt/(Ce + Pr)[b] |
|---|---|---|---|---|---|---|---|
| $Pt/CeO_2$-U | 41.4 | 0.4 | 42.3 | 15.9 | 0.0 | – | 0.026 |
| $Pt/CeO_2$-C | 30.9 | 0.9 | 48.9 | 19.4 | 0.0 | – | 0.048 |
| $Pt/CeO_2$-N | 33.5 | 0.8 | 47.2 | 18.5 | 0.0 | – | 0.045 |
| $Pt/Ce_{0.9}Pr_{0.1}O_2$-U | 43.0 | 0.2 | 37.7 | 13.8 | 5.3 | 2.60 | 0.008 |
| $Pt/Ce_{0.9}Pr_{0.1}O_2$-C | 30.8 | 0.7 | 45.9 | 16.2 | 6.5 | 2.48 | 0.031 |
| $Pt/Ce_{0.9}Pr_{0.1}O_2$-N | 30.7 | 1.1 | 46.0 | 14.9 | 7.2 | 2.08 | 0.051 |

[a] Ce/Pr nominal atomic ratio on $Pt/Ce_{0.9}Pr_{0.1}O_2$ catalysts = 9.
[b] Pt/(Ce + Pr) nominal atomic ratio = 0.009.

adsorption–desorption isotherms and XRD, respectively. Minor differences are observed in the crystallite sizes of the ceria-based supports, values ranging from 9 to 14 nm. The BET specific surface area values also fall in a narrow range (79–93 $m^2/g$) and only the $Pt/Ce_{0.9}Pr_{0.1}O_2$-N presents a lower surface area (49 $m^2/g$), which is consistent with values typically reported in the literature for Ce–Pr mixed oxides prepared by nitrate calcination [31]. The pore volumes obtained for the $Pt/CeO_2$-U and $Pt/Ce_{0.9}Pr_{0.1}O_2$-U catalysts, prepared by urea precipitation, are significantly lower than those obtained for the other catalysts, in spite of both the surface areas and crystallite size being fairly similar. The lower pore volume obtained for catalysts prepared by urea precipitation can be tentatively attributed to pore blocking by carbonate-like species, as discussed below, and/or to tight agglomeration of the primary crystallites.

The measured cell parameter values are quite similar for the catalysts, these values corresponding to those expected for a pure ceria crystal. Note that both cerium and praseodymium can adopt the +3 and +4 oxidation states, and that the cationic radii are quite similar for both elements. For this reason, a change in the cell parameter is not detected upon praseodymium doping.

Raman spectra included in Fig. 2 show a band at 450–460 $cm^{-1}$, which is ascribed to the Raman-active $F_{2g}$ mode of fluorite ceria, and another band or shoulder at 565 $cm^{-1}$ which is attributed to vacant sites created on the ceria support. The intensity of the $F_{2g}$ band diminishes while the 565 $cm^{-1}$ band increases in intensity upon ceria doping with praseodymium due to the deformation of the parent fluorite structure. In addition, fluorescence produced by praseodymium also decreases the intensity of the main $F_{2g}$ band. The creation of vacancies on the $Ce_{0.9}Pr_{0.1}O_2$ supports occurs due to the higher reducibility of the $Pr^{4+}$ cation compared to the $Ce^{4+}$ cation. It is also important to highlight that the position of the band at 450–460 $cm^{-1}$ is shifted to lower Raman shift when praseodymium is introduced in the ceria support, this also being evidence for the presence of a higher concentration of 3+ cations in the praseodymium-containing supports [31–33].

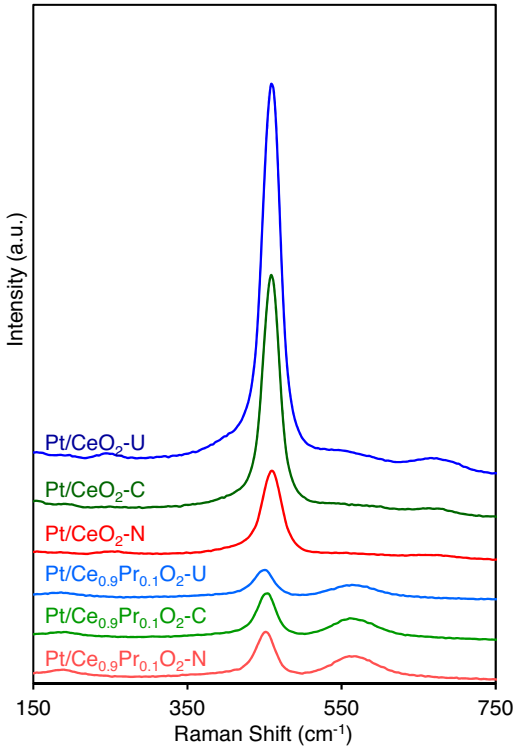


**Fig. 2.** Raman spectra of the catalysts.

### 3.2. XPS and $H_2$ chemisorption characterization

Table 3 compiles the atomic surface composition of the catalysts as determined by XPS. The Ce/Pr atomic surface ratios determined for the catalysts containing $Ce_{0.9}Pr_{0.1}O_2$ as a support are well below the nominal ratios calculated from the mixed oxide stoichiometry, evidencing the preferential accumulation of praseodymium on the surface of the particles. This has been reported by other authors and has been attributed to Pr leaching and subsequent precipitation during the noble metal impregnation step [34].

All of the catalysts present a significant amount of carbon on the surface, as expected for ceria-based materials. This carbon can be tentatively attributed to the formation of carbonate-like species upon chemisorption of atmospheric $CO_2$. The catalysts prepared by urea precipitation ($Pt/CeO_2$-U and $Pt/Ce_{0.9}Pr_{0.1}O_2$-U) contain the highest amounts of surface carbon (Table 3), and this could be one of the reasons for the lower pore volume of these catalysts (see Table 2), i.e., as a result of pore blocking. The lower pore volume of catalysts prepared by urea precipitation seems to affect the Pt dispersion, since much lower Pt/(Ce + Pr) atomic surface ratios were measured for these catalysts than for those prepared by nitrate calcination and using the activated carbon template method. Note that most Pt/(Ce + Pr) values are well above the nominal atomic ratios due to the preferential accumulation of Pt on the surface, as expected, and to the generally high Pt dispersions in the catalysts.

The lower dispersion of platinum in catalysts prepared by urea precipitation was confirmed by $H_2$ chemisorption measurements (Table 4). The lowest Pt dispersion, lowest metal surface area,

**Table 4**
Platinum dispersion, metal surface area and mean particle size determined by $H_2$ chemisorption.

| Sample | Pt dispersion (%) | Metal surface area ($m^2/g$ sample) | Mean particle diameter (nm) |
|---|---|---|---|
| $Pt/CeO_2$-U | 51 | 1.25 | 2.23 |
| $Pt/CeO_2$-C | 68 | 1.68 | 1.66 |
| $Pt/CeO_2$-N | 61 | 1.50 | 1.86 |
| $Pt/Ce_{0.9}Pr_{0.1}O_2$-U | 54 | 1.33 | 2.10 |
| $Pt/Ce_{0.9}Pr_{0.1}O_2$-C | 60 | 1.47 | 1.90 |
| $Pt/Ce_{0.9}Pr_{0.1}O_2$-N | 60 | 1.49 | 1.88 |

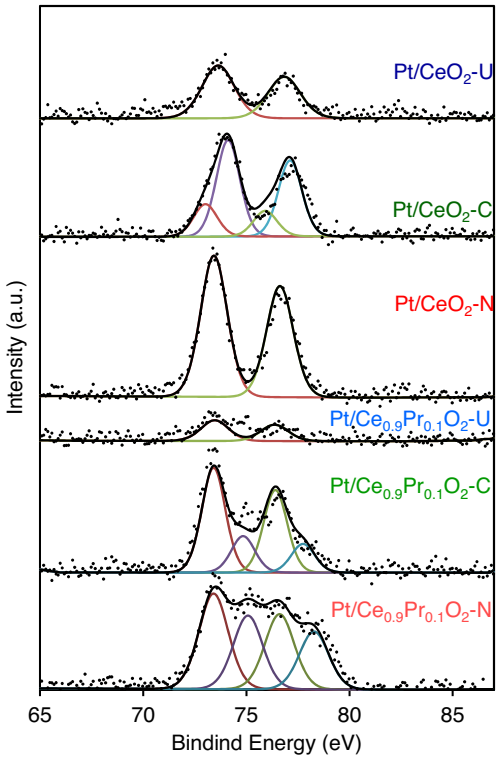


**Fig. 3.** XPS spectra of Pt 4f transitions.

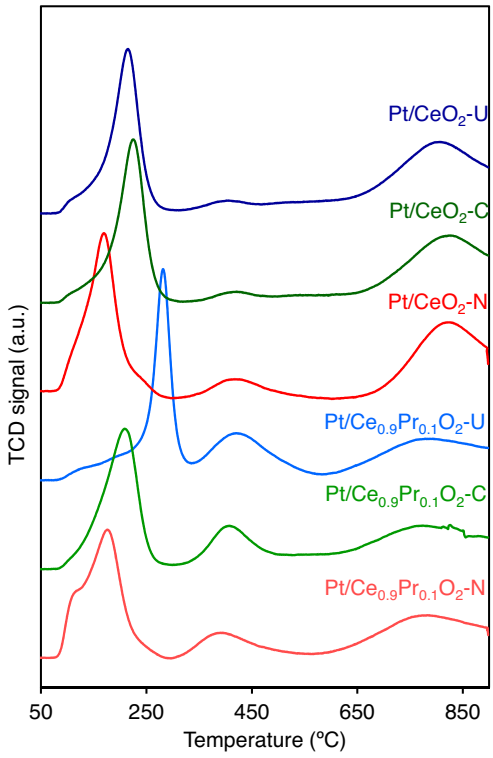


**Fig. 4.** $H_2$-TPR profiles of the catalysts.

and highest mean particle sizes correspond to $Pt/CeO_2$-U and $Pt/Ce_{0.9}Pr_{0.1}O_2$-U.

The Pt 4f spectra of the catalysts, which are included in Fig. 3, also show differences in the Pt–support interactions. Two main bands corresponding to the Pt $4f_{7/2}$ level (at lower binding energies) and Pt $4f_{5/2}$ level (at higher binding energies) are shown in Fig. 3. All of the catalysts present the main Pt $4f_{7/2}$ peak at 73.5–74.0 eV, which can be attributed to either $Pt^{2+}$ or $Pt^{4+}$ [31]. No significant differences are observed in the oxidation state of Pt or in the Pt–support interaction for catalysts containing pure ceria as the support. Only a small deconvoluted band could be inferred in the Pt 4f spectra of the $Pt/CeO_2$-C sample, prepared by the carbon template route, at lower energies with respect to the main bands. This could indicate the presence of a different platinum species.

For the Pr-containing catalysts, each Pt 4f band of the $Pt/Ce_{0.9}Pr_{0.1}O_2$-C and $Pt/Ce_{0.9}Pr_{0.1}O_2$-N catalysts can be deconvoluted into two components, and an additional band at ca. 75 eV is observed. This band can be attributed to cationic Pt with a very strong interaction with the support, that is, with a very high negative charge density transfer from the noble metal to the support. However, this effect is not observed for the other Pr-containing catalyst ($Pt/Ce_{0.9}Pr_{0.1}O_2$-U), which was prepared by urea precipitation, and this is in agreement with the higher Pt particle size and lower Pt dispersion in this catalyst.

### 3.3. $H_2$-TPR characterization

Additional information about the catalysts was obtained by $H_2$-TPR. The TCD profiles obtained in these experiments are included in Fig. 4, in which three peaks are observed for all of the catalysts, as reported in other studies [35,36]. The $H_2$ consumed above 700 °C is assigned to bulk reduction, that is, to the reduction of $Ce^{4+}$ and $Pr^{4+}$ cations located within the oxide particles. The lowest temperature peak between 75 and 350 °C, depending on the sample, is attributed to both platinum oxide reduction and noble metal-catalyzed surface reduction of the support [5,35]. The TCD signal appearing between 350 and 600 °C can be ascribed to the reduction of the support surface, but in areas which are not in close contact with platinum particles where the catalytic effect of the noble metal is less important. The decomposition of carbonates and the reduction of hydroxyl groups would also contribute to the signal in this temperature range [36,37].

From the $H_2$-TPR data it is evident that the presence of praseodymium enhances the oxygen mobility due to an effective insertion of praseodymium in the ceria structure leading to a high amount of defects. Proof of this is that the bulk reduction peaks at high temperature are not so pronounced compared with the catalysts containing pure ceria as the support.

Paying special attention to the peaks at the lowest temperature, the most reducible samples correspond to those synthesized by direct nitrate calcination ($Pt/CeO_2$-N and $Pt/Ce_{0.9}Pr_{0.1}O_2$-N), which is the simplest synthesis method of the three examined. These samples, as deduced from $H_2$ chemisorption and XPS, display high metal dispersion that facilitates a good metal–support interaction. The small shoulder detected at low temperatures for $Pt/Ce_{0.9}Pr_{0.1}O_2$-N may be evidence of better reducibility and an enhanced metal–support interaction.

### 3.4. $NO_x$ storage efficiency measurements

In order to evaluate the $NO_x$ storage properties of the samples, $NO_x$ storage efficiency measurements (NSE) were performed at 200 °C under continuously flowing lean conditions. In this context, NSE is defined as the amount of $NO_x$ stored during the lean phase divided by the total amount of $NO_x$ supplied to the catalyst during that same period. The results of these experiments are summarized in Table 1, while Table SD1 (Supplementary data) shows the cumulative amount of $NO_x$ stored on each sample in μmol/g. As shown in Table 5, for short storage times (less than 5 min), little difference in NSE is observed between the Pr-modified samples

**Table 5**
$NO_x$ storage efficiency at 200 °C measured under continuous lean conditions.

| Time (min) | $NO_x$ storage efficiency (%) | | | | | |
|---|---|---|---|---|---|---|
| | $Pt/CeO_2$-U | $Pt/CeO_2$-C | $Pt/CeO_2$-N | $Pt/Ce_{0.9}Pr_{0.1}O_2$-U | $Pt/Ce_{0.9}Pr_{0.1}O_2$-C | $Pt/Ce_{0.9}Pr_{0.1}O_2$-N |
| 1 | 86.9 | 88.9 | 96.4 | 85.8 | 93.4 | 96.8 |
| 5 | 80 | 77.5 | 97.8 | 61.4 | 78.4 | 93.8 |
| 10 | 76.5 | 69.4 | 98.3 | 48.8 | 64.3 | 86.9 |
| 30 | 66.2 | 55.9 | 94.6 | 35.1 | 47.9 | 53.8 |
| 60 | 53.7 | 47.9 | 75.3 | 31.3 | 44.4 | 42.1 |

and their $Pt/CeO_2$ analogs. Moreover, clear trends are not evident at such short times: while $Pt/Ce_{0.9}Pr_{0.1}O_2$-C shows slightly higher NSE than $Pt/CeO_2$-C, $Pt/Ce_{0.9}Pr_{0.1}O_2$-U is inferior to $Pt/CeO_2$-U, while $Pt/Ce_{0.9}Pr_{0.1}O_2$-N and $Pt/CeO_2$-N are similar. For long storage times, i.e., ≥30 min (which are of little relevance in the context of real-world applications), there is a drop in $NO_x$ storage capacity for the Pr-containing samples, no matter which preparation method was employed. This does not appear to be the consequence of differences in BET surface area, given that with the exception of $Pt/Ce_{0.9}Pr_{0.1}O_2$-N and $Pt/CeO_2$-N, the specific surface areas of the Pr-modified samples and their $Pt/CeO_2$ analogs are similar. Comparing the three different methods, the samples prepared by the nitrate calcination route exhibit consistently higher NSE values (for storage times up and including 30 min) than the samples prepared by the other two methods, although again this does not appear to be related to their specific surface areas.

Supplementary table related to this article can be found, in the online version, at http://dx.doi.org/10.1016/j.apcatb.2014.08.016.

### 3.5. Catalyst evaluation under cycling conditions

$NO_x$ storage and reduction over the samples was investigated under cycling conditions, the results being summarized in Fig. 5. The corresponding $NO_x$ concentration profiles are collected in Fig. 6. Consideration of the results included in Fig. 5 reveals a number of trends, the most striking being the superior performance exhibited by the Pr-promoted samples. Indeed, at each temperature, and for each preparation method, the cycle-averaged $NO_x$ conversion of the $Pt/Ce_{0.9}Pr_{0.1}O_2$ sample is substantially higher than that of its $Pt/CeO_2$ analog, amounting to a difference of 10–15% in the absolute $NO_x$ conversion in some cases. It is also evident that the preparation method has a significant impact on catalyst performance. At 200 and 300 °C the nitrate decomposition method affords the most active catalysts (for both $Pt/Ce_{0.9}Pr_{0.1}O_2$ and $Pt/CeO_2$ samples), while the carbon-templated samples are the least active. At 400 °C clear trends are less apparent in this respect. Also notable is the finding that $NO_x$ conversion reaches a maximum for each of the catalysts at 300 °C. In general, the $Pt/Ce_{0.9}Pr_{0.1}O_2$ and $Pt/CeO_2$ samples afford higher $NO_x$ conversion at 200 °C than 400 °C, the exception being the sample prepared by carbon templating, for which this ordering is reversed.

Further insights are provided by consideration of the $NO_x$ storage efficiency (NSE) and rich phase $NO_x$ release during cycling. As shown in Fig. 5, the trends for catalyst NSE mirror those for the $NO_x$ conversion. Indeed, it is apparent that lean phase NSE is the main determinant of the cycle-averaged $NO_x$ conversion. This follows from the fact that rich phase $NO_x$ release from the catalysts (defined as the amount of $NO_x$ released during the rich phase divided by the total amount of $NO_x$ stored during the lean phase) is relatively minor. From the data in Fig. 5 it is apparent that for all of the catalysts NSE reaches a maximum at 300 °C (of the three temperatures examined), while rich phase $NO_x$ release is at a minimum. The inferior NSE obtained at 200 °C compared to 300 °C is consistent with our previous observations for ceria-based LNT catalysts and reflects either less complete regeneration of $NO_x$ storage sites at 200 °C (compared to 300 °C) and/or a more severe kinetic limitation with respect to NO oxidation to $NO_2$ at 200 °C. Inferior $NO_x$ storage at 400 °C can be attributed to the relative thermal instability of surface cerium nitrates at this temperature, as documented in the literature [38,39].

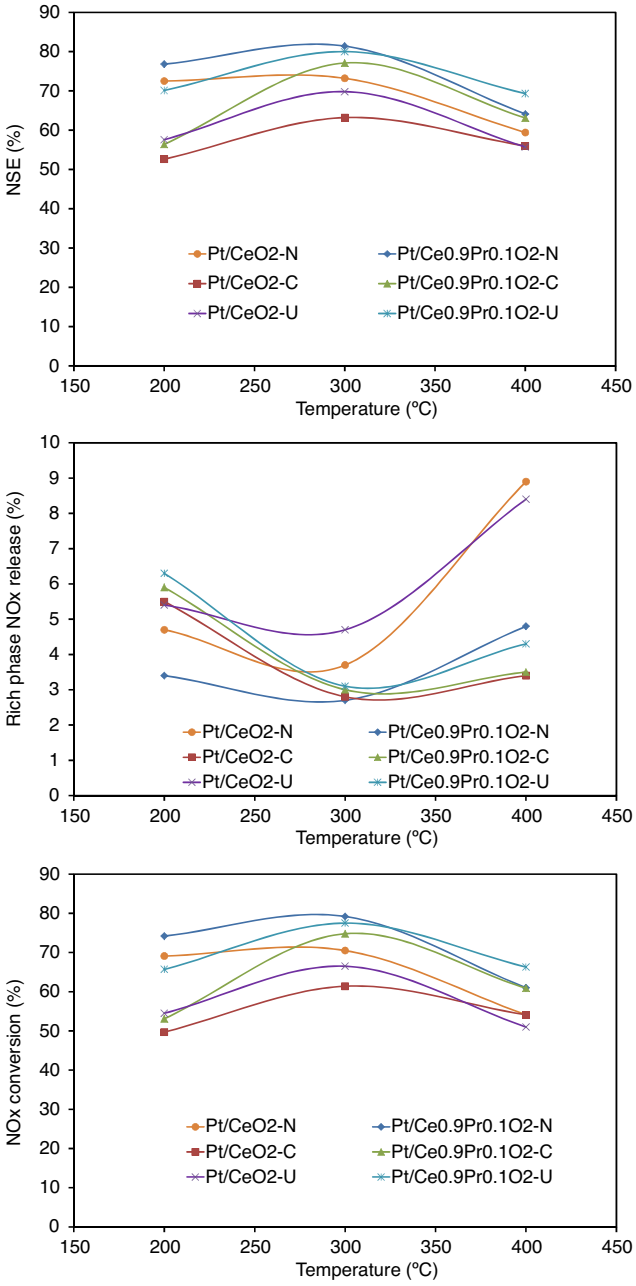


**Fig. 5.** $NO_x$ storage efficiency, rich phase $NO_x$ release and $NO_x$ conversion under lean-rich cycling conditions.

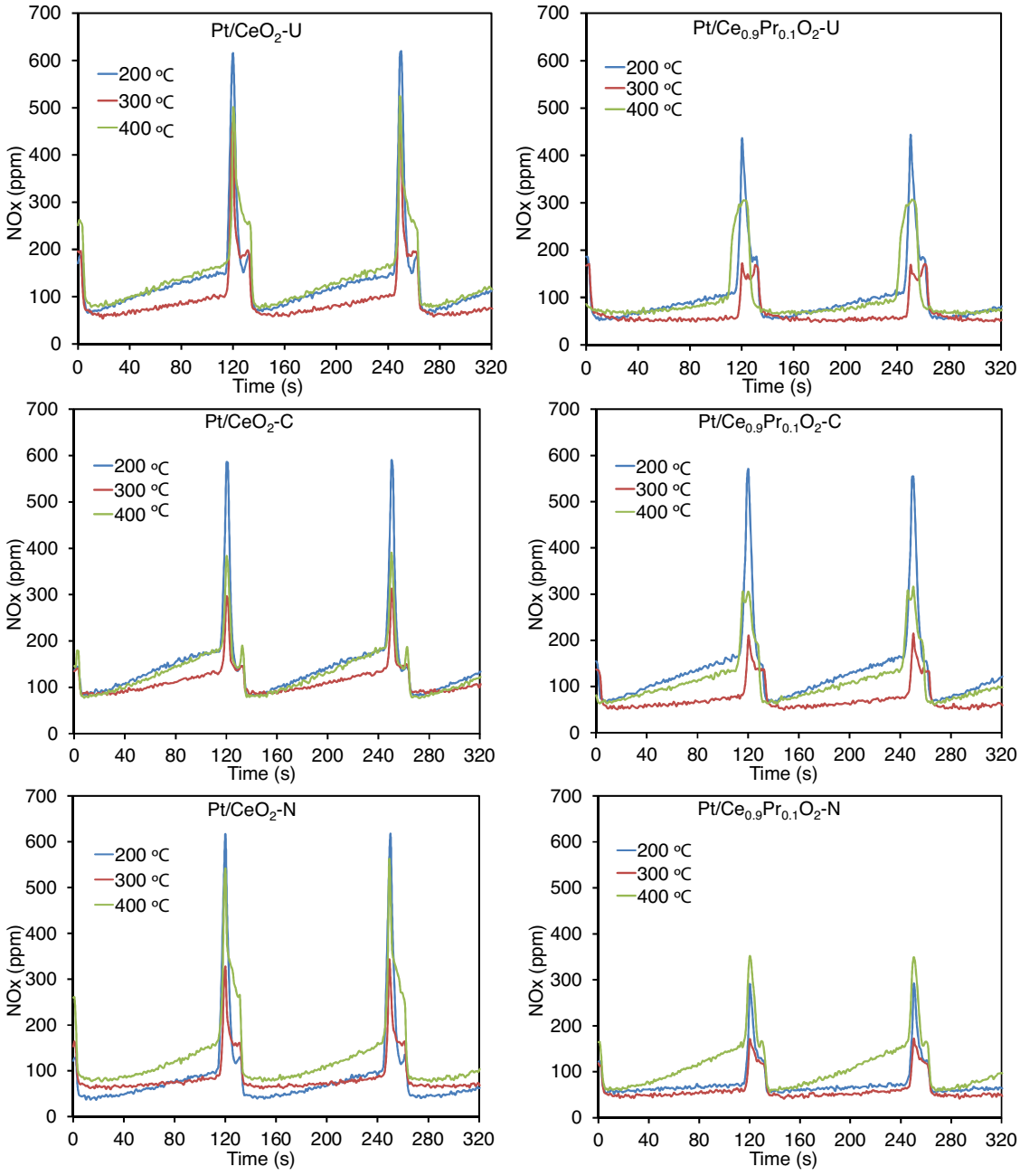


**Fig. 6.** $NO_x$ concentration profiles measured at the reactor outlet during lean-rich cycling experiments.

The observation that rich phase $NO_x$ release from the catalysts reaches a minimum at 300 °C indicates that at this temperature the kinetics of nitrate decomposition and $NO_x$ reduction are well balanced. The higher $NO_x$ release at 200 °C can be ascribed to an imbalance in these rates, i.e., the rate of $NO_x$ reduction is too slow for the liberated $NO_x$ to be fully consumed. Even though the rate of $NO_x$ reduction should be greatly increased at 400 °C, at this temperature the thermal instability of the nitrates is such that significant $NO_x$ slip occurs. Comparing the $Pt/Ce_{0.9}Pr_{0.1}O_2$ and $Pt/CeO_2$ samples, it is evident that at 300 and 400 °C the Pr-containing samples prepared by the nitrate calcination and urea routes show lower rich phase $NO_x$ release than their $Pt/CeO_2$ analogs, albeit that these effects are small. No clear tends are evident for the 200 °C data, although here too, the $Pt/Ce_{0.9}Pr_{0.1}O_2$-N sample is superior to its $Pt/CeO_2$ analog.

From the foregoing it is clear that the presence of Pr infers significant benefits with respect to $NO_x$ storage and release during lean-rich cycling, particularly lean phase NSE. It is important to realize that under cycling conditions, NSE represents the product of the "initial" or first cycle NSE (i.e., the NSE measured for a completely regenerated catalyst) and the extent to which the $NO_x$ storage sites on the catalyst are regenerated. From the NSE measurements discussed in Section 3.4, it is evident that the Pr-containing samples do not provide any benefit over their $Pt/CeO_2$ analogs with respect to the first cycle NSE. Therefore, the superior cycle-averaged NSE of the Pr-containing catalysts must derive from their ability to be more fully regenerated during rich purging.

Previous studies on the $CeO_2$–$ZrO_2$ system have shown that doping $CeO_2$ with $Zr^{4+}$, a non-reducible cation, has the effect of stabilizing adsorbed $NO_x$ [40,41]. Evidently, nitrates are more stable

on a non-reducible 4+ cation than on a reducible cation ($Ce^{3+/4+}$). It has also been observed that $CeO_2$–$ZrO_2$ doping with $Nd^{3+}$ (a +3-only cation) favors the decomposition of nitrate groups [42]. With this in mind, it can be inferred that ceria doping with $Pr^{3+/4+}$ favors nitrate decomposition on the basis that $Pr^{4+}$ is more easily reduced than $Ce^{4+}$, albeit the origin of this effect requires further clarification. Hence, in the absence of significant differences in surface area and platinum dispersion between the $Pt/Ce_{0.9}Pr_{0.1}O_2$ samples and their respective $Pt/CeO_2$ analogs, the improved NSE of the Pr-promoted samples under cycling conditions can be attributed to their greater reducibility.

As noted above, $Pt/Ce_{0.9}Pr_{0.1}O_2$-N displays superior performance at 200 and 300 °C with respect to NSE in comparison with the materials prepared by the urea and carbon-templating routes. This is a particularly encouraging result, given that the nitrate decomposition route is more straight-forward than the other preparation routes. The carbon-templating route in particular requires the use of a template which is consumed during the synthesis, while implementation of this synthesis method on a large scale would be problematical due to the exotherm associated with oxidation of the template during calcination. According to the $H_2$ chemisorption results shown in Table 4, the Pt dispersion in $Pt/Ce_{0.9}Pr_{0.1}O_2$-N is marginally higher than for the other two samples, while $H_2$-TPR results indicate that it undergoes surface reduction at slightly lower temperatures. A strong interaction between Pt and the $Ce_{0.9}Pr_{0.1}O_2$-N support (as indicated by the XPS data presented above), resulting in higher oxygen mobility and comparatively better reducibility, may therefore explain why the $Pt/Ce_{0.9}Pr_{0.1}O_2$-N sample shows superior NSE over the other Pr-containing samples.

### 3.6. DRIFTS measurements

The results of DRIFTS measurements on the samples provide further insights into the influence of Pr on $NO_x$ storage and reduction. Fig. 7 depicts the evolution of DRIFT spectra acquired for $Pt/CeO_2$-N and $Pt/Ce_{0.9}Pr_{0.1}O_2$-N during $NO_x$ storage at 200 °C. For both samples, bands appear at ~1293 $cm^{-1}$ and 1169 $cm^{-1}$ at short storage times, which may be assigned to the $\nu_{as}$ and $\nu_s$ vibrations of chelating nitrites, respectively [8,38,43]. A third band at 1558 $cm^{-1}$ can be attributed to chelating bidentate nitrates [8]. With increasing storage time the bands at ~1293 and 1169 $cm^{-1}$ tend to decrease in intensity, while strong bands grow in corresponding to bridging bidentate nitrates (1594 and 1216 $cm^{-1}$), chelating bidentate nitrates (1567 and 1245 $cm^{-1}$) and monodentate (1534 and 1275 $cm^{-1}$) nitrates. Weaker bands at 1032 and 1007 $cm^{-1}$ are also associated with the presence of these nitrate species [8]. Additionally, a weak band is observed to grow in for both samples at 1415–1428 $cm^{-1}$, which can be attributed to a linear nitrite [8,42], while other weak bands at ~1790 and ~1695 $cm^{-1}$ likely correspond to linear NO species present on defect and terrace sites of Pt particles [44]. A negative band which arises at ca. 1370 $cm^{-1}$ can be attributed to the removal of unidentate carbonate from the ceria surface. In the background spectra of both sets of catalysts, carbonate bands are observed at ca. 1467, 1365 and 1076 $cm^{-1}$ [45]. As $NO_x$ storage progresses, the adsorbed $CO_2$ is evidently displaced.

These results are consistent with the literature [8,38,43] which suggest that the "nitrite" route is an important pathway for $NO_x$ storage on ceria-based adsorbents. Previous studies have shown that $NO/O_2$ adsorption on $Pt/CeO_2$ [8,38], $Pt/Al_2O_3 + CeO_2$ [4] and $CeO_2$ itself [43] is dominated by the formation of nitrites at short exposure times, although the formed nitrites are gradually oxidized to nitrate. According to the literature [40,42,46], nitrites are formed via the interaction of NO with $Ce^{4+}$ sites:

$$Ce^{4+}\text{–}O^{2-} + NO \rightarrow Ce^{3+}\text{–}NO_2^- \quad (3)$$

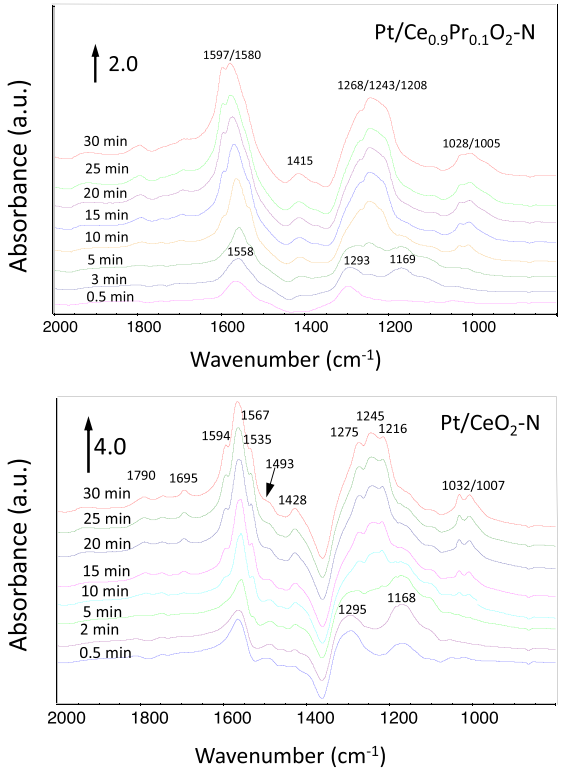


**Fig. 7.** DRIFT spectra acquired during $NO_x$ storage at 200 °C on $Pt/Ce_xPr_{1-x}O_2$-N (top) and $Pt/CeO_2$-N (bottom). Feed gas: 300 ppm NO, 5% $O_2$, Ar as balance.

$$2Ce^{4+}\text{–}OH^- + NO \rightarrow Ce^{4+}\text{–}NO_2^- + Ce^{3+}\text{–}\square + H_2O \quad (4)$$

where □ denotes a vacancy. Another potential route involves electron transfer from $Ce^{3+}$ to $NO_2$ (formed by NO oxidation on other sites) to give adsorbed $NO_2^-$:

$$Ce^{3+}\text{–}\square + NO_2 \rightarrow Ce^{4+}\text{–}NO_2^- \quad (5)$$

According to the literature, the presence of Pt is not required for these reactions to occur [40,42,46]. However, if Pt is present then it can logically fulfill two roles. First, Pt sites can chemisorb NO, which can then spill over onto the ceria surface, where reactions (3) and (4) can occur. Secondly, if oxidation of NO occurs on Pt, the thus formed $NO_2$ can react with the ceria surface to form nitrites via reaction (5). Several mechanisms have been proposed for conversion of the thus formed nitrites to nitrate [4,40,42,46], including nitrite oxidation by $NO_2$, and oxidation by an activated form of oxygen (O*); the latter can be derived either from nitrite decomposition (which affords NO and O*), or from lattice oxygen. It follows that high oxygen mobility should favor the oxidation of nitrites to more thermally stable nitrate.

Although the two sets of spectra in Fig. 7 are very similar, there are subtle differences. During $NO_x$ storage, the band at 1168 $cm^{-1}$ (chelating nitrite) is more pronounced for $Pt/CeO_2$-N than the $Pt/Ce_{0.9}Pr_{0.1}O_2$-N material (for the latter, the band is present at first but is largely gone after 5 min). Moreover, a weak band is consistently observed at 1493 $cm^{-1}$ for $Pt/CeO_2$-N, which can tentatively be assigned to a nitro-nitrite species [47]. However, this band appears to be absent in the spectra acquired for $Pt/Ce_{0.9}Pr_{0.1}O_2$-N. Based on the foregoing it can be speculated that nitrite oxidation to nitrate is a more facile process on $Pt/Ce_{0.9}Pr_{0.1}O_2$-N than on $Pt/CeO_2$-N, which is consistent with the idea that oxygen mobility should be higher in the Pr-containing catalysts.

Fig. 8 shows difference spectra acquired during subsequent reduction of the stored $NO_x$ under $H_2$. In each case the spectra were

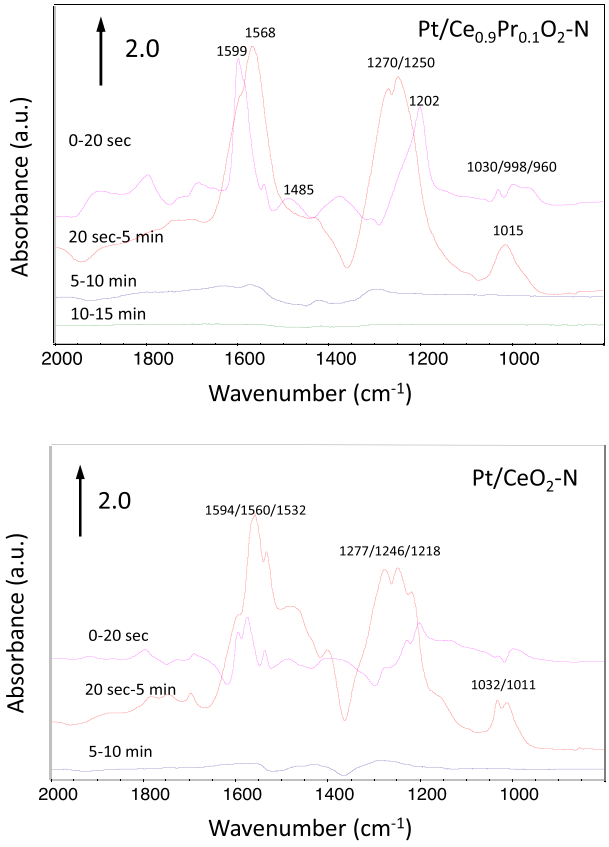


**Fig. 8.** DRIFT difference spectra showing species removed during different time periods during reduction of stored $NO_x$ at 200 °C: $Pt/Ce_xPr_{1-x}O_2$-N (top) and $Pt/CeO_2$-N (bottom). Feed gas: 1% $H_2$/Ar.

obtained by subtracting the DRIFT spectrum acquired at the end of the given period from the spectrum obtained at the start of the period, thereby revealing the species removed during the different time periods. In the case of $Pt/Ce_{0.9}Pr_{0.1}O_2$-N, a significant fraction of the nitrate species was removed in the first 20 s after switching to the rich feed gas, although a larger fraction was subsequently removed between 20 s and 5 min after the switch. After 5 min there was almost no further removal of adsorbed $NO_x$ species. In contrast, exposure of $Pt/CeO_2$-N to the rich gas resulted in relatively little removal of nitrate in the first 20 s relative to the amount removed in the 20 s to 5 min period. Comparing these two results, it follows that nitrates were removed more rapidly on $Pt/Ce_{0.9}Pr_{0.1}O_2$-N than on $Pt/CeO_2$-N. This observation can explain the superior performance of $Pt/Ce_{0.9}Pr_{0.1}O_2$-N under cycling conditions, given that faster – and hence more extensive – catalyst regeneration during rich purging results in improved $NO_x$ trapping ability in the lean phase.

## 4. Conclusions

Model $Pt/Ce_{0.9}Pr_{0.1}O_2$ NSR catalysts were prepared via several different routes, as were their $Pt/CeO_2$ analogs. Raman data indicated the presence of lattice vacancies in the $Ce_{0.9}Pr_{0.1}O_2$ supports, arising from the higher reducibility of the $Pr^{4+}$ cation compared to $Ce^{4+}$. For the $Pt/Ce_{0.9}Pr_{0.1}O_2$-N and $Pt/Ce_{0.9}Pr_{0.1}O_2$-C samples, XPS data indicated the presence of cationic Pt with a very strong interaction with the support, i.e., with a very high negative charge density transfer from the noble metal to the support. For the Pr-promoted samples, $H_2$-TPR profiles contained high temperature bulk reduction peaks which were less pronounced compared with their ceria analogs, indicating that the presence of praseodymium enhances oxygen mobility due to the creation of lattice defects.

When tested under lean-rich cycling conditions, the cycle-averaged $NO_x$ conversion of the $Pt/Ce_{0.9}Pr_{0.1}O_2$ samples was in each case substantially higher than that of the $Pt/CeO_2$ analog, amounting to a difference of 10–15% in the absolute $NO_x$ conversion in some cases. According to DRIFTS data, a double role can be assigned to Pr doping; on the one hand, Pr accelerates the oxidation of adsorbed $NO_x$ species during the lean periods. On the other hand, Pr doping destabilizes the adsorbed $NO_x$ species during the rich periods, and the kinetics of nitrate decomposition are faster on $Pt/Ce_{0.9}Pr_{0.1}O_2$ than $Pt/CeO_2$, leading to improved catalyst regeneration. Overall, these findings suggest that ceria-based mixed oxides incorporating Pr are promising materials for $NO_x$ storage–reduction catalysts, particularly for low temperature applications.

## Acknowledgments

The financial support of Generalitat Valenciana (predoctoral stay BEFPI/2012), the Spanish Ministry of Economy and Competitiveness (Project CTQ2012-30703), and co-financing by FEDER resources is acknowledged. Partial financial support was also provided by the National Science Foundation and the U.S. Department of Energy (DOE) under award no. CBET-1258742. However, any opinions, findings, conclusions, or recommendations expressed herein are those of the authors and do not necessarily reflect the views of the DOE.

## References

[1] C. Lambert, R. Hammerle, R. McGill, M. Khair, C. Sharp, SAE Technical Paper Series: Technical paper 2004-01-1292, 2004.
[2] W.S. Epling, L.E. Campbell, A. Yezerets, N.W. Currier, J.E. Parks II, Catal. Rev. Sci. Eng. 46 (2004) 163.
[3] A.F. Diwell, R.R. Rajaram, H.A. Shaw, T.J. Truex, Stud. Surf. Sci. Catal. 71 (1991) 139.
[4] X. Wang, L. Lv, Q. Zhang, Y. Zhang, J. Wang, M. Shen, Catal. Sci. Technol. 3 (2013) 200–207.
[5] C. Shi, Y. Ji, U.M. Graham, G. Jacobs, M. Crocker, Z. Zhang, Y. Wang, T.J. Toops, Appl. Catal. B 119–120 (2012) 183–196.
[6] Y. Ji, T.J. Toops, M. Crocker, Catal. Lett. 119 (2007) 257.
[7] N. Maeda, A. Urakawa, A. Baiker, J. Phys. Chem. C 113 (2009) 16724–16735.
[8] J.-Y. Luo, W.S. Epling, G. Qi, W. Li, Catal. Lett. 142 (2012) 946–958.
[9] N. Le Phuc, E.C. Corbos, X. Courtois, F. Can, P. Marecot, D. Duprez, Appl. Catal. B 93 (2009) 12.
[10] X. Wang, Y. Yu, H. He, Appl. Catal. B 104 (2011) 151–160.
[11] N. Le Phuc, X. Cortois, F. Can, S. Royer, P. Marecot, D. Duprez, Appl. Catal. B 102 (2011) 362.
[12] Y. Ren, M.P. Harold, ACS Catal. 1 (2011) 969–988.
[13] V. Easterling, Y. Ji, M. Crocker, M. Dearth, R.W. McCabe, Appl. Catal. B 123–124 (2012) 339.
[14] Y. Ji, J.S. Choi, T.J. Toops, M. Crocker, M. Naseri, Catal. Today 136 (2008) 146.
[15] J.H. Kwak, D.H. Kim, J. Szanyi, C.H.F. Peden, Appl. Catal. B 84 (2008) 545.
[16] H. Mahzoul, L. Limousy, J.F. Brilhac, P. Gilot, J. Anal. Appl. Pyrolysis 56 (2000) 179.
[17] V. Easterling, Y. Ji, M. Crocker, J. Ura, J.R. Theis, R.W. McCabe, Catal. Today 151 (2010) 338.
[18] K.M. Ryan, J.P. McGrath, R.A. Farrell, W.M. O'Neill, C.J. Barnes, M.A. Morris, J. Phys.: Condens. Matter 15 (2003) L49–L58.
[19] G. Adachi, T. Masui, in: A. Trovarelli (Ed.), Catalysis by Ceria and Related Materials, Imperial College Press, London, 2002, pp. 72–74.
[20] E. Rohart, V. Bellière-Baca, K. Yokota, V. Harlé, C. Pitois, Top. Catal. 42–43 (2007) 71.
[21] V. Rico-Perez, M. Ángeles Velasco Beltrán, Q. He, Q. Wang, C. Salinas-Martinez de Lecea, A. Bueno-Lopez, Catal. Commun. 33 (2013) 47–50.
[22] M. Schwickardi, T. Johann, W. Schmidt, F. Schüth, Chem. Mater. 14 (2002) 3913–3919.
[23] M. Crocker, U.M. Graham, R. Gonzalez, G. Jacobs, E. Morris, A.M. Rubel, R. Andrews, J. Mater. Sci. 42 (2007) 3454–3464.
[24] G. Jacobs, A.C. Crawford, B.H. Davis, Catal. Lett. 100 (2005) 147–152.
[25] C. Bueno-Ferrer, S. Parres-Esclapez, D. Lozano-Castelló, A. Bueno-López, J. Rare Earths 28 (2010) 647–653.
[26] Y. Ji, C. Fisk, V. Easterling, U. Graham, A. Poole, M. Crocker, J.-S. Choi, W. Partridge, K. Wilson, Catal. Today 151 (2010) 362–375.
[27] Parthasarathi Bera, K.C. Patil, V. Jayaram, G.N. Subbanna, M.S. Hegde, J. Catal. 196 (2000) 293–301.

[28] H.B. Yu, J.-H. Kim, H.-I. Lee, M.A. Scibioh, J. Lee, J. Han, S.P. Yoon, H.Y. Ha, J. Power Sources 140 (2005) 59–65.
[29] R.F.B. De Souza, A.E.A. Flausino, D.C. Rascio, R.T.S. Oliveira, E. Teixeira Neto, M.L. Calegaro, M.C. Santos, Appl. Catal. B 91 (2009) 516–523.
[30] Parthasarathi Bera, K.R. Priolkar, A. Gayen, P.R. Sarode, M.S. Hegde, S. Emura, R. Kumashiro, V. Jayaram, G.N. Subbanna, Chem. Mater. 15 (2003) 2049–2060.
[31] B. de Rivas, N. Guillén-Hurtado, R. López-Fonseca, F. Coloma-Pascual, A. García-García, J.I. Gutiérrez-Ortiz, A. Bueno-López, Appl. Catal. B 121–122 (2012) 162–170.
[32] M.-F. Luo, Z.-L. Yan, L.-Y. Jin, J. Mol. Catal. A 260 (2006) 157.
[33] J.R. McBride, K.C. Hass, B.D. Poindexter, W.H. Weber, J. Appl. Phys. 76 (1994) 2435.
[34] M.P. Rodríguez-Luque, J.C. Hernández, M.P. Yeste, S. Bernal, M.A. Cauqui, J.M. Pintado, J.A. Perez-Omil, O. Stephan, J.J. Calvino, S. Trasobares, J. Phys. Chem. C 112 (2008) 5900–5910.
[35] C. de Leitenburg, A. Trovarelli, J. Kaspar, J. Catal. 166 (1997) 98–107.
[36] P. Fornasiero, J. Kaspar, V. Sergo, M. Graziani, J. Catal. 182 (1999) 56–69.
[37] J.G. Nunan, M.J. Cohn, J.T. Donner, Catal. Today 14 (1992) 277–291.
[38] Y. Ji, T.J. Toops, M. Crocker, Catal. Lett. 110 (2006) 29–37.
[39] B. Azambre, I. Atribak, A. Bueno-López, A. García-García, J. Phys. Chem. C 114 (2010) 13300–13312.
[40] I. Atribak, B. Azambre, A. Bueno-López, A. García-García, Appl. Catal. B 92 (2009) 126–137.
[41] A. Bueno-Lopez, Appl. Catal. B 146 (2014) 1–11.
[42] A.M. Hernández-Giménez, L.P. dos Santos Xavier, A. Bueno-López, Appl. Catal. A 462–463 (2013) 100–106.
[43] S. Philipp, A. Drochner, J. Kunert, H. Vogel, J. Theis, E.S. Lox, Top. Catal. 30/31 (2004) 235–238.
[44] A. Bourane, O. Dulaurent, S. Salasc, C. Sarda, C. Bouly, D. Bianchi, J. Catal. 204 (2001) 77–88.
[45] T. Shido, Y. Iwasawa, J. Catal. 141 (1993) 71.
[46] B. Levasseur, A.M. Ebrahim, T.J. Bandosz, Langmuir 27 (2011) 9379–9386.
[47] K.I. Hadjiivanov, Cat. Rev. Sci. Eng. 42 (2000) 71–144.